Ultrasonics 84 (2018) 341–349

Contents lists available at ScienceDirect

Ultrasonics

journal homepage: www.elsevier.com/locate/ultras

Mode repulsion of ultrasonic guided waves in rails

Philip W. Loveday *, Craig S. Long, Dineo A. Ramatlo

Sensor Science and Technology, CSIR Material Science and Manufacturing, Box 395, Pretoria 0001, South Africa

ARTICLE INFO

Article history:
Received 18 August 2017
Received in revised form 17 November 2017
Accepted 24 November 2017
Available online 24 November 2017

Keywords:
Semi-analytical finite element method
Modes of guided wave propagation
Mode repulsion
Rail track
Symmetric structure

ABSTRACT

Accurate computation of dispersion characteristics of guided waves in rails is important during the development of inspection and monitoring systems. Wavenumber versus frequency curves computed by the semi-analytical finite element method exhibit mode repulsion and mode crossing which can be difficult to distinguish. Eigenvalue derivatives, with respect to the wavenumber, are used to investigate these regions. A term causing repulsion between two modes is identified and a condition for two modes to cross is established. In symmetric rail profiles the mode shapes are either symmetric or antisymmetric. Symmetric and antisymmetric modes can cross each other while the modes within the symmetric and antisymmetric families do not appear to cross. The modes can therefore be numbered in the same way that Lamb waves in plates are numbered, making it easier to communicate results. The derivative of the eigenvectors with respect to wavenumber contains the same repulsion term and shows how the mode shapes swop during a repulsion. The introduction of even a small asymmetry appears to lead to repulsion forces that prevent any mode crossings. Measurements on a continuously welded rail track were performed to illustrate a mode repulsion.

© 2017 Elsevier B.V. All rights reserved.

1. Introduction

Rail track inspection and monitoring systems have been developed based on guided wave ultrasound [1]. These systems operate at frequencies where dozens of guided wave modes can propagate. Some of these modes can propagate large distances (1 – 2 km) making it possible to monitor a long section of rail from a single transducer location. In addition to being multi-modal, signals can exhibit significant dispersion. Modelling of the wave propagation characteristics is required during the development of these systems and is also used in the analysis of signals obtained. As the rail has a complex cross-section, numerical modelling is required and the semi-analytical finite element (SAFE) method is used by various research groups. This method is very powerful for constant cross-section waveguides such as rail. Dispersion characteristics can be computed from the SAFE model at discrete wavenumbers or discrete frequencies. The behaviour of a selected mode of propagation is often required over a range of frequencies and it is then necessary to track this mode from one solution frequency to the next. This need arises in a number of situations including: designing a transducer to excite a particular mode; computing the reflection, transmission and mode coupling of selected modes by a defect or when performing phased array signal processing to preferentially transmit and receive selected mode combinations over the range of frequencies included in the excitation signal.

Dispersion curves, computed by the SAFE method, can show sudden deviations as two modes approach each other. In some cases the wavenumber versus frequency curves for two modes cross each other but in other cases they converge and then suddenly diverge without crossing. Sometimes it is difficult to determine whether two modes have crossed or not and this makes it difficult to track a particular mode. Similar behaviour has been observed for Lamb waves in plates and this mode repulsion was analysed by Überall et al. [2] who showed that repulsion occurs between modes within the symmetric or antisymmetric families but that dispersion curves of symmetric and antisymmetric modes cross each other.

The SAFE method produces a system of equations of motion and an eigenvalue problem is solved to compute the frequencies and mode shapes. The repulsion and crossing of wavenumber versus frequency curves for rail models is investigated in this paper by analysing the second derivative of the eigenvalues with respect to wavenumber and the first derivative of the eigenvectors with respect to wavenumber. Rail is manufactured to be symmetric and is modelled as such. Wear that occurs in use will generally not be symmetric and the influence of the introduction of a small asymmetry is investigated.

In Section 2 the SAFE analysis is briefly described before the eigenvalue problem is presented. A repulsion region and a crossing region in a symmetric rail model are investigated in Section 3 by analysing the second derivative of the eigenvalue with respect to

* Corresponding author.
E-mail address: ploveday@csir.co.za (P.W. Loveday).

https://doi.org/10.1016/j.ultras.2017.11.014
0041-624X/© 2017 Elsevier B.V. All rights reserved.

wavenumber. A small asymmetry is then introduced and analysed in the same regions. Section 4 describes an experimental measurement performed to illustrate a mode repulsion.

2. Safe modelling of guided wave propagation

The propagation of guided waves in one-dimensional waveguides of arbitrary but constant cross-section may be modelled efficiently by using the semi-analytical finite element (SAFE) method. The SAFE method uses finite element discretization over the cross-section of the waveguide and includes the wave propagation along the waveguide analytically in the element formulation. The method is relatively simple to implement and has become popular for modelling guided wave propagation in rails [3–8].

In the formulation presented by Gavric [5] the displacement field (u, v, w) was chosen to take the form:

$$\begin{aligned} u(x,y,z,t) &= u(x,y)\cdot e^{-j(\kappa z-\omega t)} \\ v(x,y,z,t) &= v(x,y)\cdot e^{-j(\kappa z-\omega t)} \\ w(x,y,z,t) &= w(x,y)\cdot e^{-j(\kappa z-\omega t-\pi/2)} \\ &= j\cdot w(x,y)\cdot e^{-j(\kappa z-\omega t)}, \end{aligned}$$

where, z is the coordinate in the direction along the waveguide, κ the wavenumber and ω the frequency. $u(x,y)$, $v(x,y)$ and $w(x,y)$ are the interpolated displacements in the x, y and z directions respectively.

Application of the finite element method produces a system of equations of motion, which for free vibration are:

$$M\ddot{U} + [\kappa^2\cdot K_2 + \kappa\cdot K_1 + K_0]U = 0. \tag{2}$$

The equations of motion are similar to those obtained using conventional three-dimensional finite elements except for the presence of stiffness matrices that are proportional to the wavenumber and the square of the wavenumber respectively. In this formulation the mass (M) and stiffness (K_0, K_1, K_2) matrices are all real and symmetric. If we consider free harmonic vibration we obtain the eigenvalue problem:

$$[\kappa^2\cdot K_2 + \kappa\cdot K_1 + K_0]\psi = \lambda M\psi. \tag{3}$$

The propagating modes may be computed by setting the wavenumber, κ to a real value and solving the eigenvalue problem to obtain eigenvalues λ and mode shapes ψ of the propagating modes and this method is used in this paper. The frequencies ω are then computed from the eigenvalues using $\lambda = \omega^2$.

Although not used here, it is also possible to set the frequency, add an identity to the eigenvalue problem and compute the wavenumbers and mode shapes at the specified frequency [6].

An analytical expression for the group velocity is obtained by differentiating the solution of the eigenvalue problem with respect to frequency,

$$v_g = \frac{\partial\omega}{\partial\kappa} = \frac{\partial\omega}{\partial\lambda}\frac{\partial\lambda}{\partial\kappa} = \frac{1}{2\omega}\frac{\psi^T[2\kappa K_2 + K_1]\psi}{\psi^T M\psi}. \tag{4}$$

Eqs. (3) and (4) were used to compute the dispersion characteristics for a UIC60 profile rail section (with Young's modulus of 206 GPa, Poisson's ratio of 0.3 and density of 7800 kg/m^3) as shown in Fig. 1.

From Fig. 1 we see that when wavenumber – frequency dispersion curves approach they sometimes appear to cross each other while other times they appear to approach closely and then diverge. When this repulsion occurs it is often easier to observe in the group velocity curves. To further investigate this behaviour we study the derivatives of the eigenvalues and the eigenvectors in the next section.

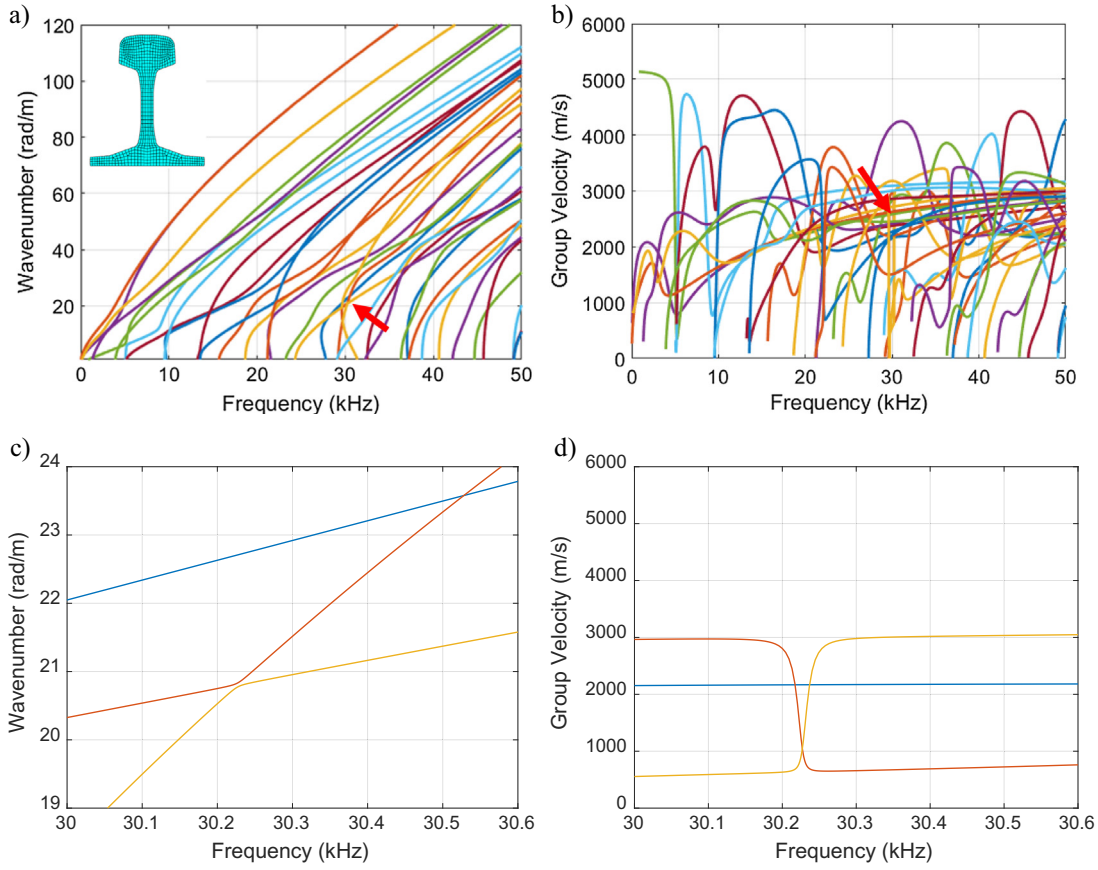

Fig. 1. SAFE mesh and computed wavenumber (a) and group velocity dispersion curves (b), with zoomed views of curves for three modes in (c) and (d).

3. Analysis of mode repulsion and mode crossing

Consider two curves approaching as we increase wavenumber. We can compute the derivatives of the eigenvalues λ with respect to wavenumber κ and also the derivatives of the eigenvectors ψ with respect to wavenumber.

The first derivatives of the eigenvalues and eigenvectors for a system with symmetric mass and stiffness matrices were derived by Fox and Kapoor [9]. Two methods of calculating the derivatives of the eigenvectors were presented. The second method is used in Appendix A where the first derivatives of the eigenvalues and eigenvectors and the second derivative of the eigenvalue are

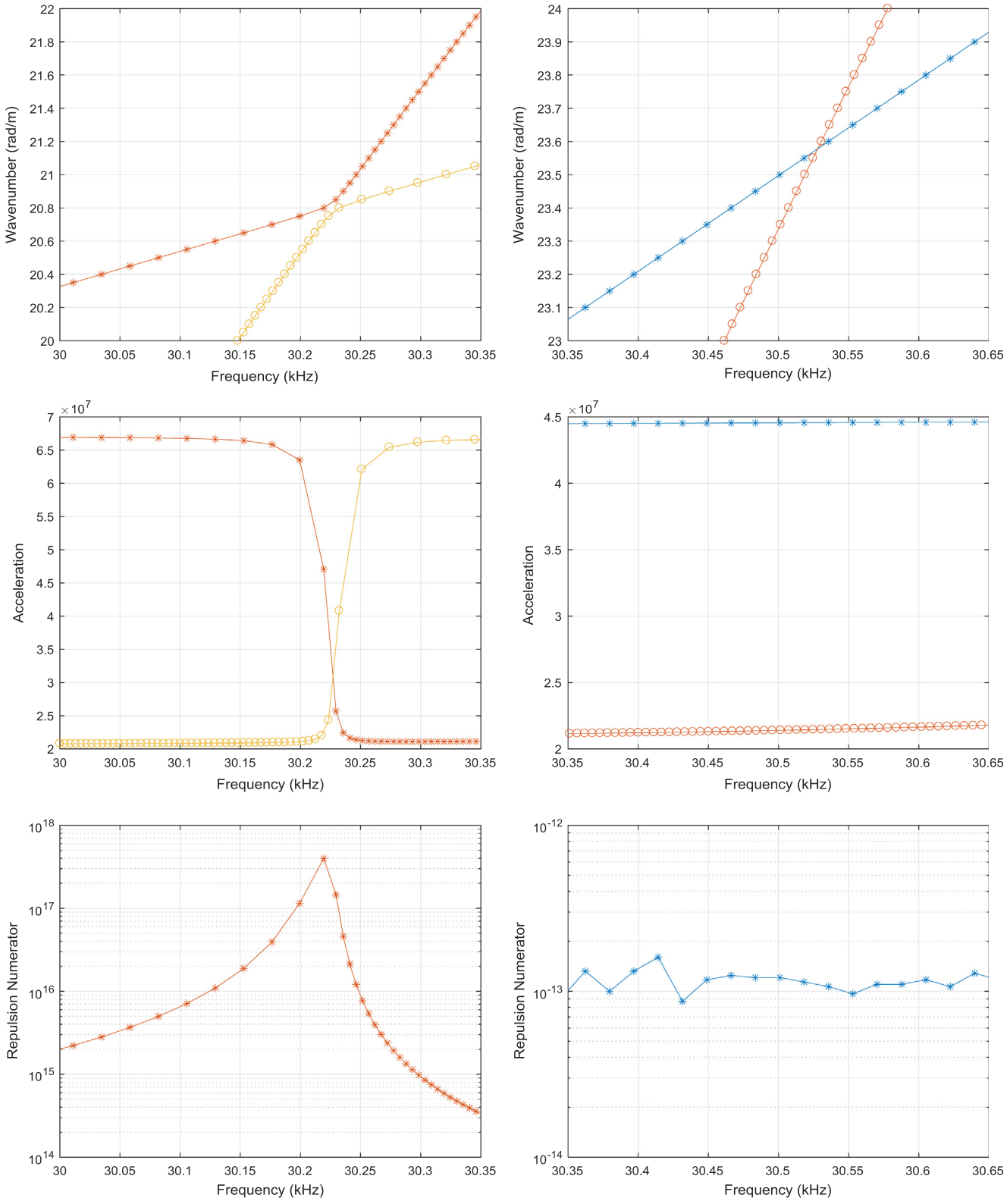

Fig. 2. Mode Repulsion (left) and Mode Crossing (right) in a Symmetric Rail Model.

derived for the SAFE eigenvalue problem. The results are stated here and then discussed.

The first derivative of the kth eigenvalue with respect to the wavenumber is denoted $\dot{\lambda}_k$ and is:

$$\dot{\lambda}_k = \frac{\psi_k^T \dot{K} \psi_k}{\psi_k^T M \psi_k}, \tag{5}$$

where, $K = [\kappa^2 \cdot K_2 + \kappa \cdot K_1 + K_0]$ and $\dot{K} = [2\kappa \cdot K_2 + K_1]$.

We note that this is similar to the expression for the group velocity in equation 4 and the group velocity can easily be derived from this expression. If we assume that the eigenvectors are scaled so that $\phi_i^T M \phi_i = 1$, the first derivative of the eigenvector with respect to the wavenumber is:

$$\dot{\phi}_k = \sum_{i \neq k} \frac{\phi_i^T \dot{K} \phi_k}{(\lambda_k - \lambda_i)} \phi_i. \tag{6}$$

The second derivative of an eigenvalue with respect to wavenumber is:

$$\ddot{\lambda}_k = \phi_k^T \ddot{K} \phi_k + 2 \sum_{i \neq k} \frac{\left(\phi_i^T \dot{K} \phi_k\right)^2}{(\lambda_k - \lambda_i)}. \tag{7}$$

An analogous equation, for the standard eigenvalue problem, was described by Tao in a blog [10] who explained that the terms on the right hand side of Eq. (7) may be viewed as various 'forces' acting on the eigenvalue. The first term $\phi_k^T \ddot{K} \phi_k$ contains the acceleration of the stiffness matrix, while the second term $2\sum_{i \neq k} \frac{(\phi_i^T \dot{K} \phi_k)^2}{(\lambda_k - \lambda_i)}$ is a repulsive force. As with Newton's third law the force exerted by eigenvalue λ_i on eigenvalue λ_k is equal and opposite to the force eigenvalue λ_k exerts on eigenvalue λ_i. As two eigenvalues approach the denominator in the repulsion 'force' decreases and becomes zero if the eigenvalues cross. Therefore the only way two eigenvalues can cross is if the numerator of the repulsion 'force' is zero. We can therefore state that for two wavenumber versus frequency curves to cross it is necessary that $\phi_i^T \dot{K} \phi_k = 0$ as the modes approach. We have noticed that mode crossing occurs when one mode shape is symmetric and the other is antisymmetric. In Appendix B we follow the approach of Wang et al. [11] where a symmetric structure is considered to be two separate half structures with appropriate displacement constraints on the shared plane to show that the numerator will be zero when a symmetric mode approaches an antisymmetric mode.

Note that Eq. (6) for the eigenvectors has a similar form to the second term in Eq. (7) and if the numerator is zero there will be no repulsion. If there is repulsion, this equation shows how one mode shape influences the mode shape evolution of the second mode and vice versa when two eigenvalues approach.

These equations provide a mathematical explanation of mode repulsion. Überall et al. [2] illustrated that the nature of the Lamb waves in plates switch between being predominantly compression or shear as the dispersion curves pass through a repulsion region. The mode shapes in the rail are more complex and it was not possible to identify such a general change in nature.

3.1. Symmetric rail profiles

The mode repulsion and mode crossing shown in Fig. 1(c) are analysed further in Fig. 2. The acceleration and repulsion forces for the two modes in a repulsion region and a crossing region were computed using a model of a symmetric rail. We see that when repulsion occurs the numerator of the repulsion term is non zero while when a symmetric mode and an antisymmetric mode cross the repulsion term is effectively zero. Evaluating this term would provide one method of determining whether a repulsion will occur or not.

The evolution of two symmetric mode shapes in a repulsion region is illustrated in Fig. 3. We see that while the wavenumber curves do not cross, the mode shapes effectively swop as the curves pass through the repulsion region. Inside the repulsion region the mode shapes are each approximately a linear combination of the mode shapes outside of the repulsion region. This repulsion region was selected for illustration of the phenomenon because it will be studied experimentally in Section 4.

The ideal rail profile is symmetric about the vertical axis. Similar to the case of finite structures analysed by Wang et al. [11], the mode shapes of distinct modes of a symmetric structure are either symmetric or antisymmetric. Where multiple modes have the same frequency and wavenumber (at a crossing point) the mode shapes are a linear combination of symmetric and antisymmetric mode shapes. This fact was used by Ryue et al. [8] who model only half of the rail cross-section and apply appropriate boundary conditions to calculate the symmetric modes and then a second set of boundary conditions to compute the antisymmetric modes. Because the two models are solved separately it is expected that there can be no repulsion between symmetric and antisymmetric modes. If the complete rail cross-section is modelled we can post process the mode shapes to determine if the modes are symmetric or antisymmetric. The dispersion curves shown in Fig. 1a and b were divided into sets of symmetric and antisymmetric modes and are plotted separately in Fig. 4.

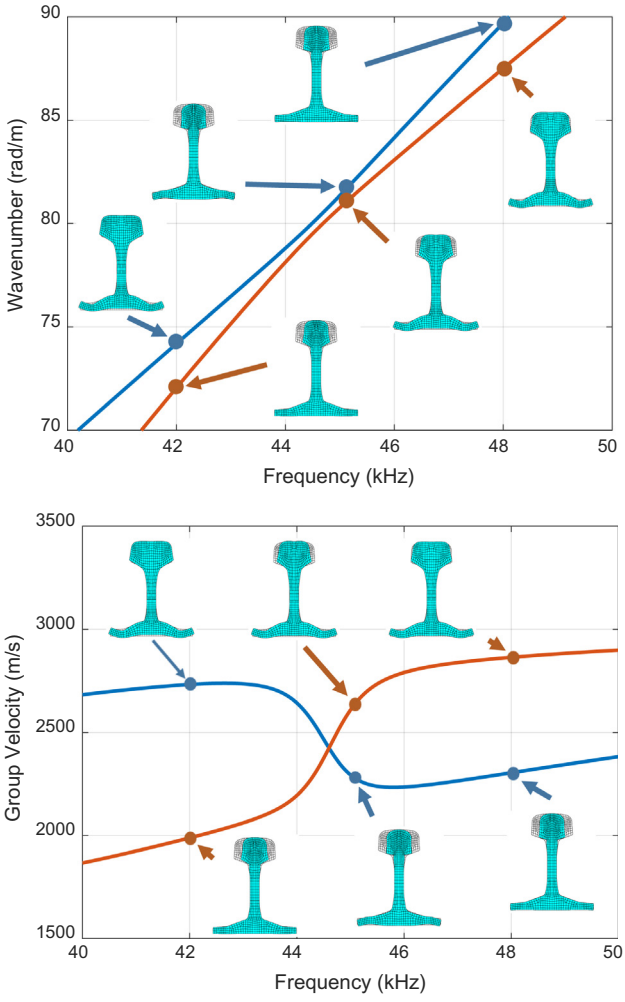

Fig. 3. Dispersion curves for a mode repulsion of two symmetric mode shapes with mode shapes computed at 42, 45 and 48 kHz.

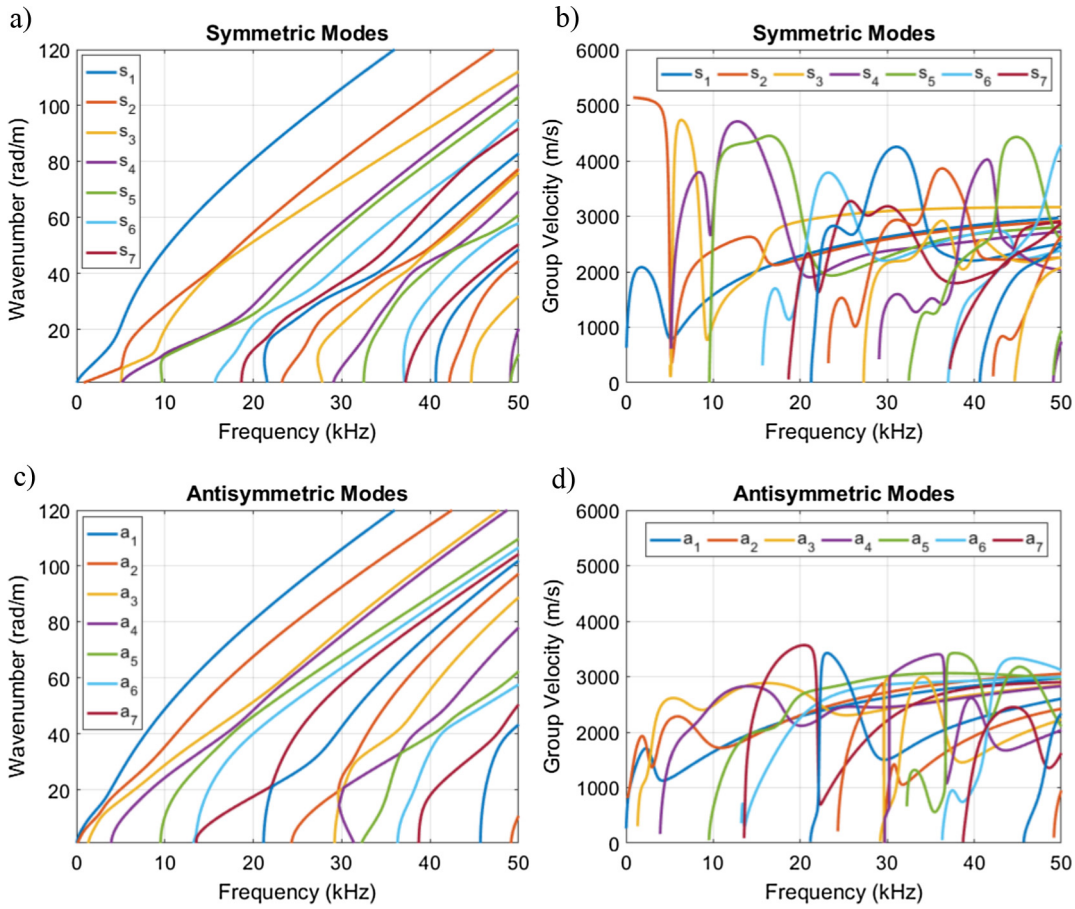

Fig. 4. Computed dispersion curves for symmetric (a & b) and antisymmetric (c & d) modes.

The curves in Fig. 4 were generated using small steps in wavenumber. Zooming in on the curves in Fig. 4a and c shows that the wavenumber – frequency curves for the modes within each family do not cross each other. Instead the modes approach and then repel each other. When this happens we see that the group velocity curves of the two modes cross each other and appear to then continue as though they have swopped. The behaviour of the symmetric and antisymmetric dispersion curves and modes appears to be analogous to that of the symmetric and antisymmetric Lamb waves in plates [2]. The fact that the wavenumber dispersion curves within the symmetric and antisymmetric mode families do not cross means that it is not necessary to track the modes to generate the curves. Similar to Lamb waves, the modes can be numbered in a simple manner at any frequency in order of decreasing wavenumber as s_1, s_2, s_3 ... and a_1, a_2, a_3 ... for the two families. The same numbering is obtained if the modes are numbered as they cut on. With such a numbering system it is possible to communicate precisely which modes you are referring to and it is no longer necessary to attempt to describe the mode shape in words. The first seven symmetric and antisymmetric modes are numbered in this manner in Fig. 4.

It may be possible to find a symmetric structure in which two symmetric or two antisymmetric modes cross if the eigenvector pair satisfy the condition $\phi_i^T \dot{K} \phi_k = 0$ (are $\dot{K}$ orthogonal). We believe that such a situation is highly unlikely and we have not observed such a situation in the rail profiles we have analysed.

3.2. Influence of rail asymmetry on dispersion behaviour

While rails are manufactured to be symmetric the wear that occurs is generally not symmetric. To investigate the influence of rail asymmetry we introduce gauge corner wear by increasing the gauge corner radius by 2 mm. The relatively small change to the mesh is shown in Fig. 6.

The wavenumber, acceleration and repulsion force numerator for the repulsion and crossing regions analysed previously (in Fig. 2) are plotted for the asymmetric rail model in Fig. 5. The repulsion in the symmetric model remains a repulsion in the asymmetric model and it appears that the wavenumber curves now approach each other more closely before diverging. The former crossing has become a very clear repulsion due to the introduction of the asymmetry.

The dispersion curves were inspected up to 50 kHz and it was observed that all the previous crossings between symmetric and antisymmetric modes in the symmetric model have become repulsion points in the asymmetric model. This is illustrated for two crossings in the symmetric model in Fig. 6. At the first crossing modes a_9 and s_{10} crossed in the symmetric model while modes m_{18} and m_{19} repel in the asymmetric model. At the second crossing modes a_{10} and s_{10} crossed in the symmetric model while modes m_{20} and m_{19} repel in the asymmetric model.

4. Measurement of guided wave repulsion

Measurements were performed on an operational rail track to detect a mode repulsion. The repulsion shown in Fig. 3 was selected for experimental measurement because this repulsion involves a mode that has little motion in the foot of the rail and it is therefore expected that this mode will have relatively low attenuation and be detectable over large distances, making dispersion easier to observe. The measurement was performed by bonding a small piezoelectric sandwich transducer to the outside

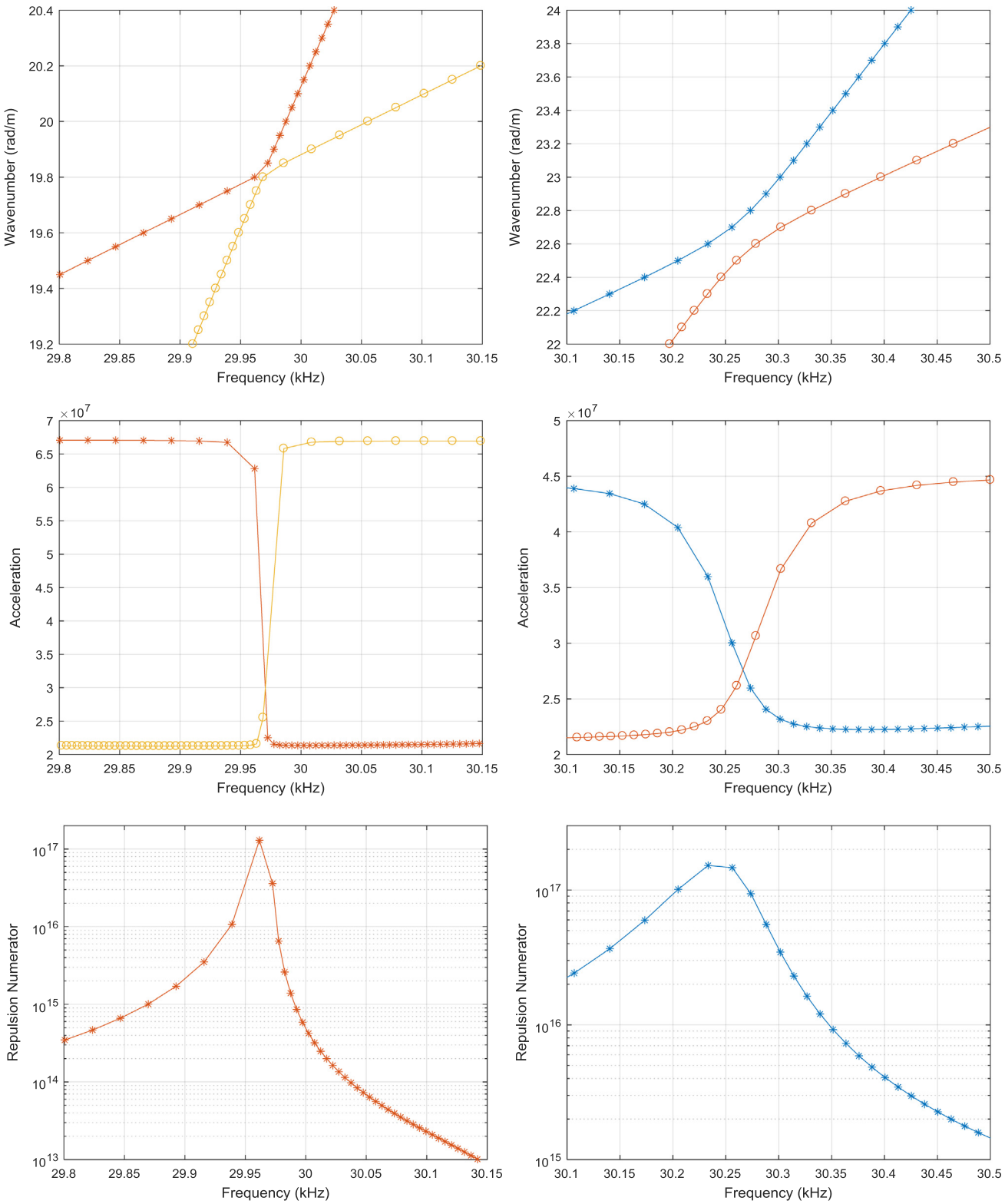

Fig. 5. Mode repulsion in a rail with asymmetry.

surface of the rail head and performing a pulse – echo measurement. A 17 cycle tone burst signal with 45 kHz centre frequency was used to drive the transducer and the response at the transducer was measured. The continuously welded rail contains aluminothermic welds at regular intervals and the weld caps of these welds cause multiple reflections and mode coupling of the guided wave modes. The spectrogram shown in Fig. 7a shows the result of a short-time Fourier transform of part of the measured signal. A reflector was then added to the rail at a distance of approximately 220 m from the transducer. The reflector was actually a second sandwich transducer glued to the outside of the rail head. The measurement was repeated and additional reflected

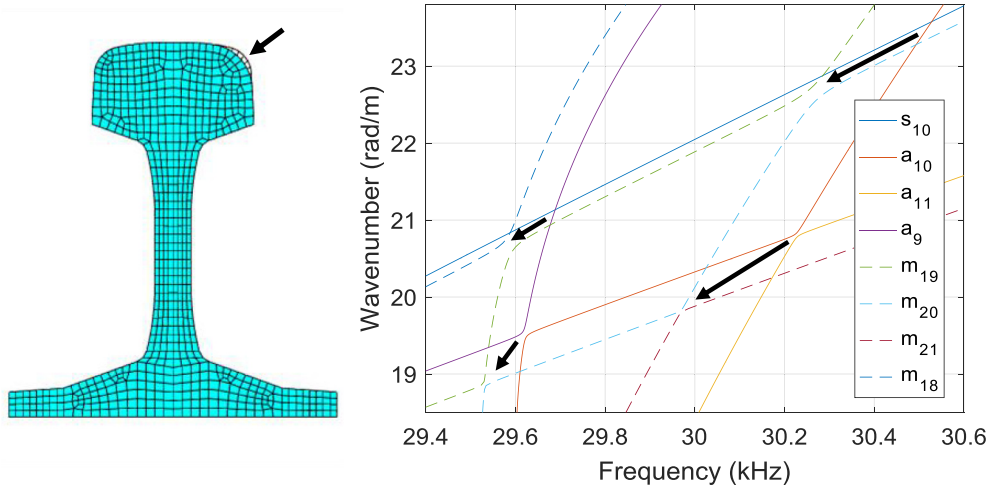

Fig. 6. Mode crossings in symmetric model become mode repulsions when asymmetry is introduced in the geometry.

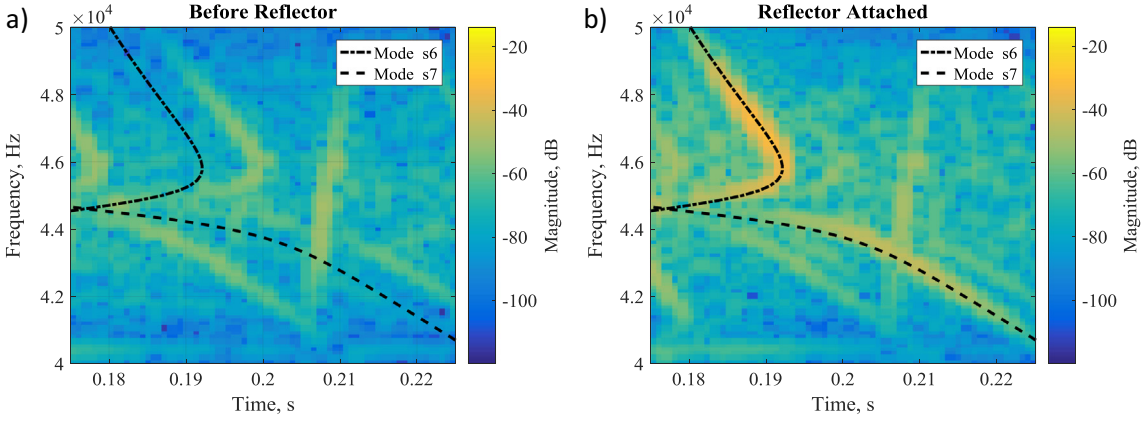

Fig. 7. Measured spectrograms (a) without reflector, (b) with reflector and superimposed SAFE computed arrival times.

energy is evident in the spectrogram shown in Fig. 7b. This is due to the guided waves being reflected by the added reflector and returning to the pulse-echo transducer. The distance travelled to the reflector and back to the pulse-echo transducer was divided by the group velocities of the two modes (shown in Fig. 3) and superimposed on the spectrograms in Fig. 7. The shape of these curves show good agreement with the shape of the experimental dispersion in Fig. 7b. Only the parts of the group velocity curves with the lower group velocity could be detected experimentally because the mode shapes for the remainder on the group velocity curves contain motion of the foot of the rail and are attenuated. The transducer location was chosen to excite and sense the mode shapes with relatively low attenuation.

5. Conclusions

The mode repulsion and crossing behaviour of approaching wavenumber versus frequency curves was studied by analysing the second derivative of the eigenvalue with respect to wavenumber. A term describing the repulsion force between two eigenvectors was obtained. A condition for this force to be zero and for mode crossing to occur was identified. If this condition is not satisfied the repulsion force is inversely proportional to the distance between the eigenvectors, which prevents mode crossing and a mode repulsion occurs. The derivative of the eigenvectors contains the same condition and shows how the mode shapes swop during a repulsion.

In a symmetric rail model there is no repulsion force between symmetric and antisymmetric modes and these will cross. Similar to Lamb waves in plates it appears that two modes within either the symmetric or antisymmetric families of modes do not cross each other. Symmetric and antisymmetric modes can therefore be numbered by adopting the numbering convention used for modes in plates.

If a small asymmetry is introduced in the rail profile there are no longer symmetric and antisymmetric modes and all modes appear to repel. No mode crossing was observed in this case.

An experimental measurement was performed on a rail track and a predicted repulsion behaviour was observed. Damping was present in the measured rail track but was not included in the analysis. The influence of different damping models on the mode repulsion behaviour could be investigated in future.

Appendix A. Derivatives of eigenvalues and eigenvectors

This derivation follows that in [9]. Because the mass and stiffness matrices are symmetric we can write solutions to Eq. (3) as;

$$K\psi_k = \lambda_k M\psi_k, \tag{A1a}$$

$$\psi_k^T K = \lambda_k \psi_k^T M, \text{ or} \tag{A1b}$$

$$\psi_k^T K\psi_k = \lambda_k \psi_k^T M\psi_k. \tag{A1c}$$

If we differentiate Eq. (A1b) with respect to the wavenumber we obtain:

$$\dot{K}\psi_k + K\dot{\psi}_k = \dot{\lambda}_k M\psi_k + \lambda_k M\dot{\psi}_k. \tag{A2}$$

We pre-multiply (A2) by ψ_k^T and use (A1c) to obtain an expression for the first derivative of the eigenvalue with respect to the wavenumber:

$$\dot{\lambda}_k = \frac{\psi_k^T \dot{K}\psi_k}{\psi_k^T M\psi_k}. \tag{A3}$$

We note that this is similar to the expression for the group velocity and the group velocity can easily be derived from this expression.

To obtain an expression for the first derivative of the eigenvector with respect to the wavenumber we note that the eigenvectors span the vector space and we can use them as a basis for the derivatives:

$$\dot{\psi}_k = \sum_{i=1}^{N} a_{ki}\psi_i. \tag{A4}$$

We can find the coefficients a_{ki} by substituting (A4) into (A2) and pre-multiplying by ψ_i^T to obtain, $\psi_i^T\dot{K}\psi_k + \psi_i^T K\sum_{i=1}^{N} a_{ki}\psi_i = \dot{\lambda}_k\psi_i^T M\psi_k + \lambda_k\psi_i^T M\sum_{i=1}^{N} a_{ki}\psi_i$, and use the mass and stiffness orthogonality of the eigenvectors to simplify this equation for the case when $i \neq k$,

$$\psi_i^T\dot{K}\psi_k + a_{ki}\psi_i^T K\psi_i = \lambda_k a_{ki}\psi_i^T M\psi_i \quad , \quad i \neq k.$$

Using (A1c) we can obtain the expression for a_{ki}:

$$a_{ki} = \frac{\psi_i^T\dot{K}\psi_k}{(\lambda_k - \lambda_i)\psi_i^T M\psi_i}. \tag{A5}$$

To find the coefficient a_{kk} we differentiate the expression $\psi_k^T M\psi_k = c$ to obtain $\dot{\psi}_k M\psi_k + \psi_k M\dot{\psi}_k = 0$ and after substituting (A4) we find that $a_{kk} = 0$. Therefore we have the expression for the derivatives of the eigenvectors.

$$\dot{\psi}_k = \sum_{i\neq k} \frac{\psi_i^T\dot{K}\psi_k}{(\lambda_k - \lambda_i)\psi_i^T M\psi_i}\psi_i. \tag{A6}$$

To simplify the derivation of the second derivatives of the eigenvalues we scale the eigenvectors so that $\phi_i^T M\phi_i = 1$, and write A6 as

$$\dot{\phi}_k = \sum_{i\neq k} \frac{\phi_i^T\dot{K}\phi_k}{(\lambda_k - \lambda_i)}\phi_i. \tag{A7}$$

From (A3), $\dot{\lambda}_k = \phi_k^T\dot{K}\phi_k$ and differentiation yields:

$$\ddot{\lambda}_k = \dot{\phi}_k^T\dot{K}\phi_k + \phi_k^T\ddot{K}\phi_k + \phi_k^T\dot{K}\dot{\phi}_k.$$

Substituting (A7) and manipulating provides the expression for the second derivative of an eigenvalue with respect to wavenumber,

$$\ddot{\lambda}_k = \phi_k^T\ddot{K}\phi_k + 2\sum_{i\neq k} \frac{\left(\phi_i^T\dot{K}\phi_k\right)^2}{(\lambda_k - \lambda_i)}. \tag{A8}$$

Appendix B. Repulsion between symmetric and antisymmetric modes

The first derivative of the eigenvector and the second derivative of the eigenvalue both contain the term $\phi_i^T\dot{K}\phi_k$.

We consider a symmetric structure and investigate this term when one eigenvector is symmetric and the other is antisymmetric.

We follow the approach of [11] and consider the symmetric structure to be made up of two separate halves with the one being the mirror reflection of the other and with appropriate boundary conditions between the two structures on the symmetry plane. The symmetry plane is the *yz* plane and the *x* direction is reversed in the two halves as shown in Fig. B1. After discretization using the SAFE method the eigenvalue problem for the combined system may be written as:

$$\begin{bmatrix} K & \\ & K \end{bmatrix}\begin{Bmatrix} u_1 \\ u_2 \end{Bmatrix} = \lambda\begin{bmatrix} M & \\ & M \end{bmatrix}\begin{Bmatrix} u_1 \\ u_2 \end{Bmatrix}, \tag{B1}$$

where, u_1 and u_2 are displacement vectors for substructures 1 and 2 respectively along with the boundary conditions,

$$J_1 u_1 = -J_1 u_2 \text{ on } x = 0 \tag{B2a}$$

$$J_2 u_1 = J_2 u_2 \text{ on } x = 0, \tag{B2b}$$

on the plane of symmetry. The first boundary condition (B2a) forces the displacements in the *x* direction on the common boundary to be equal but in opposite direction as the *x* axes are in opposite directions in the two substructures. The second boundary condition (B2b) forces the displacements in the *y* and *z* directions on the common boundary to be equal.

Wang et al. used the fact that any displacement field in the symmetric structure can be written as a combination of a symmetric and an antisymmetric displacement field and that this decouples the equations of motion and the boundary conditions. The eigenvalue problem for one substructure can then be solved twice, firstly with symmetric boundary conditions and then with antisymmetric boundary conditions to obtain the symmetric modes and the antisymmetric modes respectively. Therefore any eigenvector (mode shape), of a symmetric structure, is either symmetric or antisymmetric or if there are repeated eigenvalues the corresponding eigenvectors can be written as linear combinations of symmetric and antisymmetric eigenvectors.

If we write a symmetric eigenvector of the two substructures as $\begin{Bmatrix} \phi_s \\ \phi_s \end{Bmatrix}$ and an antisymmetric eigenvector as $\begin{Bmatrix} \phi_a \\ -\phi_a \end{Bmatrix}$ then the repulsion numerator term for a combination of a symmetric and antisymmetric mode is $\begin{Bmatrix} \phi_s \\ \phi_s \end{Bmatrix}^T\begin{bmatrix} \dot{K} & \\ & \dot{K} \end{bmatrix}\begin{Bmatrix} \phi_a \\ -\phi_a \end{Bmatrix}$. It is clear that this term is zero and repulsion will not occur between a symmetric mode and an antisymmetric mode.

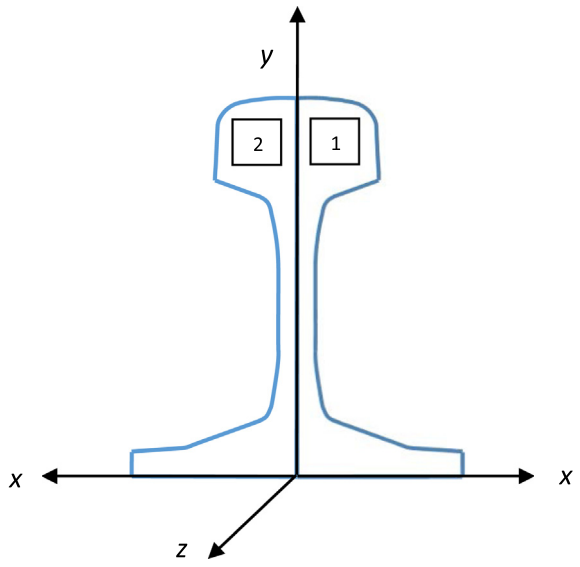

Fig. B1. Symmetric structure and coordinate system adapted from Wang et al. [11].

References

[1] P.W. Loveday, Guided wave inspection and monitoring of railway track, J. Nondestr. Eval. 31 (4) (2012) 303–309, https://doi.org/10.1007/s10921-012-0145-9.

[2] H. Überall, B. Hosten, M. Deschamps, A. Gerard, Repulsion of phase-velocity dispersion curves and the nature of plate vibrations, J. Acoust. Soc. Am. 96 (2) (1994) 908–917, https://doi.org/10.1121/1.411434.

[3] I. Bartoli, A. Marzani, F. Lanza di Scalea, E. Viola, Modeling wave propagation in damped waveguides of arbitrary cross-section, J. Sound Vib. 295 (3–5) (2006) 685–707, https://doi.org/10.1016/j.jsv.2006.01.021.

[4] V. Damljanović, R.L. Weaver, Propagating and evanescent elastic waves in cylindrical waveguides of arbitrary cross section, J. Acoust. Soc. Am. 115 (4) (2004) 1572, https://doi.org/10.1121/1.1687424.

[5] L. Gavric, Computation of propagative waves in free rail using a finite element technique, J. Sound Vib. 185 (3) (1995) 531–543, https://doi.org/10.1006/jsvi.1995.0398.

[6] T. Hayashi, W.-J. Song, J.L. Rose, Guided wave dispersion curves for a bar with an arbitrary cross-section, a rod and rail example, Ultrasonics 41 (3) (2003) 175–183. https://doi.org/doi:10.1016/S0041-624X(03)00097-0.

[7] P.W. Loveday, Semi-analytical finite element analysis of elastic waveguides subjected to axial loads, Ultrasonics 49 (3) (2009) 298–300, https://doi.org/10.1016/j.ultras.2008.10.018.

[8] J. Ryue, D. Thompson, P. White, Investigations of propagating wave types in railway tracks at high frequencies, J. Sound Vib. 315 (1–2) (2008) 157–175, https://doi.org/10.1016/j.jsv.2008.01.054.

[9] R.L. Fox, M.P. Kapoor, Rates of change of eigenvalues and eigenvectors, AIAA J. 6 (12) (1968) 2426–2429.

[10] T. Tao, When are eigenvalues stable? https://terrytaowordpress.com/2008/10/28/when-are-eigenvalues-stable/, 2008 (accessed 07.06.2017).

[11] D. Wang, C. Zhou, J. Rong, Free and forced vibration of repetitive structures, Int. J. Solids Struct. 40 (20) (2003) 5477–5494, https://doi.org/10.1016/S0020-7683(03)00279-8.